

Accurate PRD modeling of the forward-scattering Hanle effect in the chromospheric Ca I 4227 Å line

Luca Belluzzi^{1,2,3}, Simone Riva², Gioele Janett^{1,2}, Nuno Guerreiro^{1,2}, Fabio Riva^{1,2}, Pietro Benedusi^{2,4}, Tanausú del Pino Alemán^{5,6}, Ernest Alsina Ballester^{5,6}, Javier Trujillo Bueno^{5,6,7}, and Jiří Štěpán⁸

¹ Istituto ricerche solari Aldo e Cele Daccò (IRSOL), Faculty of informatics, Università della Svizzera italiana, Locarno, Switzerland

² Euler Institute, Università della Svizzera italiana, Lugano, Switzerland

³ Institut für Sonnenphysik (KIS), Freiburg i. Br., Germany

⁴ Simula Research Laboratory, Oslo, Norway

⁵ Instituto de Astrofísica de Canarias, La Laguna, Tenerife, Spain

⁶ Departamento de Astrofísica, Universidad de La Laguna, La Laguna, Tenerife, Spain

⁷ Consejo Superior de Investigaciones Científicas, Spain

⁸ Astronomical Institute ASCR, Ondřejov, Czech Republic

e-mail: luca.belluzzi@irsol.usi.ch

April 2, 2024

ABSTRACT

Context. Measurable linear scattering polarization signals have been predicted and detected at the solar disk center in the core of chromospheric lines. These forward-scattering polarization signals, which are of high interest for magnetic field diagnostics, have always been modeled either under the assumption of complete frequency redistribution (CRD), or taking partial frequency redistribution (PRD) effects into account under the angle-averaged (AA) approximation.

Aims. This work aims at assessing the suitability of the CRD and PRD-AA approximations for modeling the forward-scattering polarization signals produced by the presence of an inclined magnetic field, the so-called forward-scattering Hanle effect, in the chromospheric Ca I 4227 Å line.

Methods. Radiative transfer calculations for polarized radiation are performed in semi-empirical 1D solar atmospheres, out of local thermodynamic equilibrium (LTE). A two-step solution strategy is applied: the non-LTE RT problem is first solved considering a multilevel atom and neglecting polarization phenomena. The same problem is then solved including polarization and magnetic fields, considering a two-level atom and keeping fixed the population of the lower level calculated at the previous step. The problem of step two is linear and it is solved with a preconditioned FGMRES iterative method. The emergent fractional linear polarization signals calculated under the CRD and PRD-AA approximations are analyzed and compared to those obtained by modeling PRD effects in their general angle-dependent (AD) formulation.

Results. With respect to the PRD-AD case, the CRD and PRD-AA calculations significantly underestimate the amplitude of the line-center polarization signals produced by the forward-scattering Hanle effect.

Conclusions. The results of this work suggest that a PRD-AD modeling is required in order to develop reliable diagnostic techniques exploiting the forward-scattering polarization signals observed in the Ca I 4227 Å line. These results need to be confirmed by full 3D calculations including non-magnetic symmetry-breaking effects.

Key words. Magnetic fields – Polarization – Radiative transfer – Scattering – Sun: chromosphere

1. Introduction

When observed in quiet or moderately active regions of the solar disk, many lines of the solar spectrum, from the near infrared to the far ultraviolet, show measurable linear polarization signals, produced by the scattering of anisotropic radiation (e.g., Stenflo & Keller 1997; Gandorfer 2000, 2002, 2005; Kano et al. 2017; Rachmeler et al. 2022). These scattering polarization signals are receiving increasing attention by the scientific community because they encode precious information on the thermodynamic and magnetic properties of the solar atmosphere (e.g., Trujillo Bueno & del Pino Alemán 2022, and references therein).

When observed with low spatio-temporal resolution, scattering polarization signals are generally strongest at the edge of the solar disk (limb) and decrease towards the disk center, where they typically vanish. Consistently with this observational evidence, it can be theoretically shown that in a setting with cylin-

dric symmetry around the vertical, the amplitude of scattering polarization scales as $(1 - \mu^2)$, with μ the cosine of the inclination of the line-of-sight with respect to the vertical (e.g., Landi Degl’Innocenti & Landolfi 2004).¹ On the other hand, if the problem is not axially symmetric, non-negligible scattering polarization signals can also be obtained at $\mu = 1$, and thus also at the solar disk center, in a forward-scattering geometry (Trujillo Bueno 2001). The first detection of forward-scattering polarization on the Sun was achieved by Trujillo Bueno et al. (2002) while observing a quiescent filament in the He I 10830 Å triplet. Shortly afterward, while pointing an active region, Stenflo (2003) detected a forward-scattering signal in the chromospheric Ca I line at 4227 Å. Other remarkable disk-center observations in this line were carried out by Bianda et al. (2011) us-

¹ We note that μ also corresponds to the cosine of the heliocentric angle of the observed region.

ing the Zurich Imaging Polarimeter (ZIMPOL-III, Ramelli et al. 2010).

A lack of axial symmetry in the solar atmosphere, capable of producing forward-scattering polarization, can be due to (i) horizontal inhomogeneities in the density and temperature of the solar plasma (Manso Sainz & Trujillo Bueno 2011), (ii) spatial gradients of the plasma bulk velocity (e.g., Štěpán & Trujillo Bueno 2016; del Pino Alemán et al. 2018), and (iii) a deterministic magnetic field inclined with respect to the vertical (Trujillo Bueno 2001; Trujillo Bueno et al. 2002). In the first two scenarios, the signals are produced by a lack of axial symmetry in the radiation field that illuminates the atoms; in the third one, generally referred to as forward-scattering Hanle effect, they arise directly from the magnetic field. In general, these symmetry-breaking effects operate simultaneously, and the individual contributions can hardly be isolated. Interestingly, radiative transfer (RT) calculations carried out in state-of-the-art 3D models of the solar atmosphere, in the limit of complete frequency redistribution (CRD), show that the forward-scattering signals produced by the symmetry breaking effects (i) and (ii) are reduced by the presence of magnetic fields (Štěpán & Trujillo Bueno 2016; del Pino Alemán et al. 2018; Jaume Bestard et al. 2021). Moreover, it can be argued that the inherent averaging happening in observations with low spatio-temporal resolution significantly conceals the impact of mechanisms (i) and (ii), and indeed it is currently rather challenging to detect forward-scattering polarization signals in very quiet solar regions. As a matter of fact, the aforementioned observations in the Ca I 4227 Å line were all performed in relatively strongly magnetized regions (i.e., with noticeable V/I signals), suggesting that the forward-scattering Hanle effect might be the main mechanism responsible for their generation. To routinely detect forward-scattering polarization signals in quiet solar regions is one of the challenges for the new generation of large-aperture solar telescopes, such as DKIST (Rimmele et al. 2020) and the future EST (Quintero Noda et al. 2022).

In order to interpret the available observational data, various theoretical works have already been carried out on the modeling of forward-scattering polarization signals in the chromospheric Ca I 4227 Å line. Anusha et al. (2011) modeled the observations of Bianda et al. (2011) in 1D semi-empirical solar atmospheric models, taking partial frequency redistribution (PRD) effects into account under the angle-average (AA) approximation (see Bommier 1997b, Sect. 4.3). Their work allowed inferring information on the magnetic fields of the low chromosphere, and showed that various observed features cannot be reproduced if the CRD limit is considered. Subsequently, Carlin & Bianda (2016, 2017) modeled the Ca I 4227 forward-scattering polarization signals in 3D models of the solar atmosphere, in the limit of CRD. Their calculations neglected both the effects of horizontal RT (i.e., they considered the so-called 1.5D approximation) and the horizontal component of the model's bulk velocity. This work highlighted the key role played by the dynamics and temporal evolution of the chromospheric plasma during the integration time of the observations. In the investigations mentioned so far, the symmetry-breaking mechanisms (i) and (ii) were not taken into account. By contrast, Jaume Bestard et al. (2021) investigated the polarization of the Ca I 4227 Å line performing full 3D calculations in realistic models of the solar atmosphere with the radiative transfer code PORTA (Štěpán & Trujillo Bueno 2013) under the assumption of CRD. Accounting for all symmetry-breaking effects, their study showed that the spatial gradients in the horizontal component of the plasma bulk ve-

locity can produce conspicuous forward-scattering polarization signals, comparatively larger than those produced by horizontal inhomogeneities in the solar plasma, and that these signals are reduced by the presence of a magnetic field.

So far, all the theoretical investigations on the forward-scattering polarization of the Ca I 4227 Å line have been carried out either in the limit of CRD or considering PRD effects under the AA simplifying approximation. This is ultimately due to the formidable computational complexity of modeling scattering polarization while accounting for PRD phenomena in their most general angle-dependent (AD) formulation. Performing RT calculations in realistic atmospheric models, taking AD PRD effects into account, is today feasible (e.g., del Pino Alemán et al. 2020; Benedusi et al. 2023), and a series of 1D applications to Ca I 4227 have been presented (e.g., Janett et al. 2021a; Riva et al. 2023; Guerreiro et al. 2024). However, none of these works specifically investigated the forward-scattering Hanle effect. The present study focuses on this effect and aims at assessing the suitability of the CRD and PRD-AA approximations for its modeling in the Ca I 4227 Å line.

The article is organized as follows: Section 2 exposes the considered RT problem for polarized radiation and the adopted solution strategy. In Sect. 3, we report and analyze the emergent fractional linear polarization of the Ca I 4227 line, comparing CRD, PRD-AA, and PRD-AD calculations. Section 4 discusses the main results and their implications, while Sect. 5 provides remarks and conclusions.

2. Problem formulation and solution strategy

The Ca I line at 4227 Å is produced by the transition between the ground level of neutral calcium, $4s^2\ ^1S_0$, and the excited level $4s4p\ ^1P_1^o$. In quiet regions close to the solar limb, this line shows a large scattering polarization signal, characterized by broad lobes in the wings and a sharper peak in the core (e.g., Gandorfer 2002). Both the line-core peak and the wing lobes are sensitive to the magnetic field, the former through the Hanle effect (which only operates in the line-core region, e.g., Landi Degl'Innocenti & Landolfi 2004) and the latter through magneto-optical effects (Alsina Ballester et al. 2018). In low-resolution observations, the forward-scattering polarization signals detected close to the disk center consist instead in a single peak in the line-core region (e.g., Bianda et al. 2011). A correct modeling of the scattering polarization profiles of this line, and in particular of the wing lobes, requires taking PRD effects into account (e.g., Faurobert 1988). Nonetheless, the limit of CRD can be used to approximately model the line-core peak, in both limb and forward-scattering geometries (e.g., Sampoorana et al. 2010; Jaume Bestard et al. 2021).

The scattering polarization signal of the Ca I 4227 Å line can be suitably modeled considering a two-level atom. Indeed, the line is not part of a multiplet (the upper and lower levels have spin zero) and, since the upper level is not connected to lower-energy levels other than the ground level, its population is mainly determined by this line itself (assuming that the ionization fraction is known). In this work, we account for PRD effects using the redistribution matrix for a two-level atom with unpolarized and infinitely-sharp lower level as derived by Bommier (1997a,b). The long-lived ground level of neutral calcium can indeed be treated as infinitely sharp and, having total angular momentum $J = 0$, it cannot carry atomic polarization. The redistribution matrix is given by the sum of two terms: one that describes scattering processes that are coherent in the atomic

reference frame (R^{II}), and the other describing scattering processes that are totally incoherent in the same reference frame (R^{III}). In the observer's reference frame, we consider the exact AD expression of R^{II} , while we make the assumption of totally incoherent scattering for R^{III} (e.g., Bommier 1997b; Sampoorana et al. 2017; Riva et al. 2023). The CRD modeling is instead performed by applying the theoretical approach described in Landi Degl'Innocenti & Landolfi (2004).

In this work, we only focus on the forward-scattering Hanle effect, neglecting the two other mechanisms (i) and (ii). We thus consider the static 1D semi-empirical atmospheric model *C* of Fontenla et al. (1993, hereafter FAL-C), and we analyze the impact of inclined deterministic magnetic fields. The intensity and polarization profiles of the emergent radiation are calculated by solving the non-LTE RT problem for polarized radiation. The adopted solution strategy requires two steps: first, we solve the non-LTE RT problem neglecting polarization phenomena. This first step is carried out using the RH code (Uitenbroek 2001), and considering an atomic model for calcium composed of 25 levels (including five levels of Ca II and the ground level of Ca III). Second, we solve the non-LTE RT problem including polarization, but keeping fixed the population of the lower level calculated in step 1, so that the problem is linear (e.g., Janett et al. 2021b). This is achieved with a preconditioned FGMRES (Flexible Generalized Minimal RESidual) iterative method, as described in Benedusi et al. (2021, 2022) and Janett et al. (2024). All the physical and numerical parameters are the same as in Guerreiro et al. (2024).

3. Results

This section presents the results of our calculations of the linear scattering polarization profiles of the Ca I line at 4227 Å both in the absence and in the presence of magnetic fields. The problem is formulated in a right-handed Cartesian coordinate system with the z -axis directed along the vertical, and the x -axis directed so that the line-of-sight (LOS) lies in the $x-z$ plane ($x > 0$, $z > 0$ quadrant). The LOS is thus fully specified by the cosine of its inclination θ with respect to the vertical, that is $\mu = \cos(\theta) \in [0, 1]$. The reference direction for positive Stokes Q is taken parallel to the y -axis. The magnetic field vector is specified by the intensity B , the inclination θ_B with respect to the vertical, and the azimuth χ_B measured on the $x-y$ plane, counter-clockwise (for an observer at $z > 0$) from the x -axis. In Sect. 3.1, we analyze the case of horizontal (i.e., $\theta_B = \pi/2$) magnetic fields, while the case of non-horizontal inclined magnetic fields (i.e., $\theta_B = \pi/4$) is considered in Sect. 3.2.

3.1. Horizontal magnetic fields

Figure 1 shows the center-to-limb variation of the amplitude of the line-center scattering polarization Q/I (upper panel) and U/I (lower panel) signals of the Ca I 4227 Å line, resulting from CRD, PRD-AA, and PRD-AD calculations. As expected, in the absence of magnetic fields (dotted curves), the amplitude of the Q/I peak monotonically decreases while moving from the limb towards the disk center, where it vanishes. The U/I signal is always zero, consistently with our choice of the reference direction for positive Stokes Q . For any limb distance, the largest signals are obtained in the PRD-AD setting.

The presence of a height-independent horizontal ($\theta_B = \pi/2$, $\chi_B = 0$) magnetic field of 20 G produces a significant Hanle rotation at the limb. This leads to a depolarization of the line-

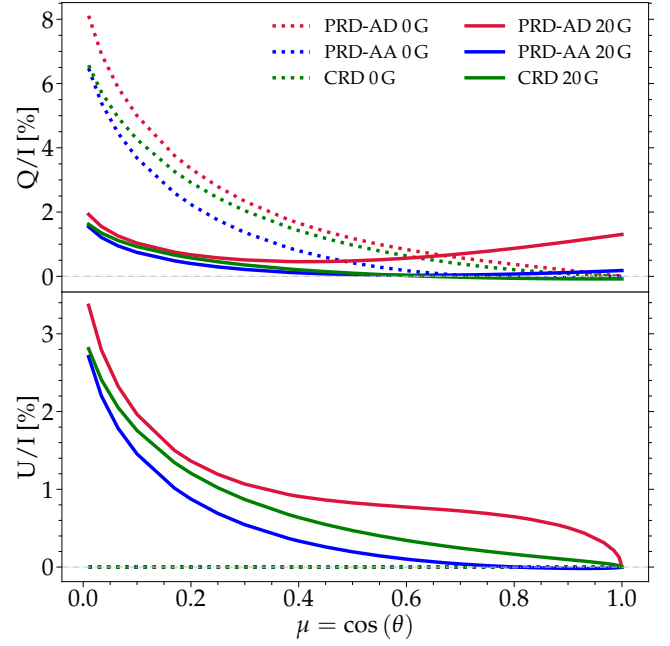


Fig. 1. Center-to-limb variation of the Ca I 4227 line-center fractional linear polarization Q/I (upper panel) and U/I (lower panel), obtained from CRD, PRD-AA, and PRD-AD calculations in the FAL-C atmospheric model, both in the absence (dotted curves) and in the presence (solid curves) of a magnetic field. The dotted curves for U/I are equal to zero. In the magnetic case, a height-independent horizontal ($\theta_B = \pi/2$, $\chi_B = 0$) magnetic field of 20 G is considered. The reference direction for positive Stokes Q is parallel to the y -axis of the considered reference system, that is perpendicular to the magnetic field.

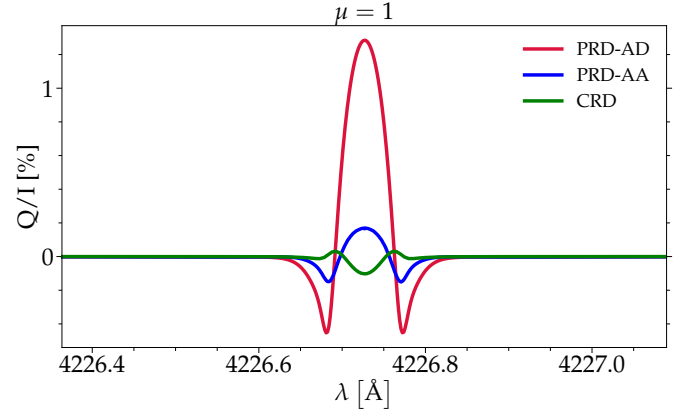


Fig. 2. Emergent Q/I profiles of Ca I 4227 at $\mu = 1$, obtained from CRD, PRD-AA, and PRD-AD calculations in the FAL-C atmospheric model, in the presence of a height-independent horizontal ($\theta_B = \pi/2$, $\chi_B = 0$) magnetic field of 20 G. The reference direction for positive Stokes Q is parallel to the y -axis of the considered reference system, that is, perpendicular to the magnetic field. In this geometry, the U/I profile vanishes, and it is thus omitted.

center Q/I signal while giving rise to an appreciable U/I signal (see solid curves). At the solar disk center, the forward-scattering Hanle effect yields a non-zero Q/I signal, while U/I is zero, consistently with the geometry of the problem. The CRD, PRD-AA, and PRD-AD calculations show significant differences for all μ , in both Q/I and U/I , with the PRD-AD results always showing the largest signal. A very interesting finding is that the PRD-AD

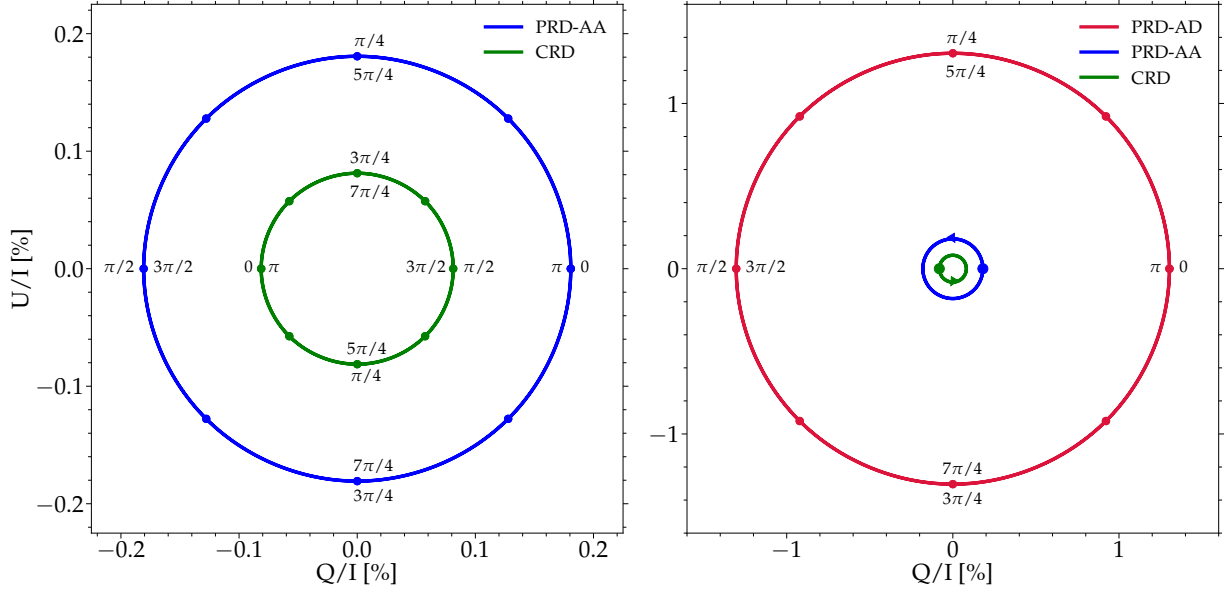


Fig. 3. Polarization diagrams of the Ca I 4227 line-center emergent radiation at $\mu = 1$, obtained from CRD, PRD-AA, and PRD-AD calculations in the FAL-C atmospheric model, in the presence of a height-independent horizontal ($\theta_B = \pi/2$) magnetic field of 20 G. The circular markers indicate the effective calculations, carried out for the azimuths $\chi_B = n\pi/8$ (with $n = 0, \dots, 15$). *Left panel:* comparison between CRD and PRD-AA calculations. *Right panel:* comparison between CRD, PRD-AA, and PRD-AD calculations (in the PRD-AA and CRD diagrams the circular marker indicates a magnetic field direction with azimuth $\chi_B = 0$, whereas the arrow refers to $\chi_B = \pi/4$). The reference direction for positive Stokes Q is parallel to the y -axis of the considered reference system.

results for Q/I drift away from the others while approaching the disk center. At $\mu = 1$, the PRD-AD signal is well above 1%, that is one order of magnitude larger than in the PRD-AA and CRD cases. Moving from the limb to the disk center, the Q/I signal obtained from PRD-AA and PRD-AD calculations first decreases, reaches a minimum, and then increases, always remaining positive. On the contrary, in the CRD case, it shows a sign reversal at around $\mu \approx 0.6$ and then remains negative until $\mu = 1$, with amplitudes always below 0.1% (see also Fig. 2). We note that the differences between PRD-AA and PRD-AD calculations in Fig. 1 are magnified by the AA approximation in the line-core of Q/I and U/I for $\mu \neq 1$, both in the absence and presence of magnetic fields (see Janett et al. 2021a). To better visualize the impact of the different scattering modelings on the forward-scattering Hanle effect signal, Fig. 2 shows the emergent Q/I profiles at $\mu = 1$. This clearly highlights the significantly stronger polarization signals resulting from PRD-AD calculations.

Figure 3 compares the polarization diagrams for the line-center radiation emitted at $\mu = 1$, obtained with PRD-AD, PRD-AA and CRD calculations, considering height-independent horizontal (i.e., $\theta_B = \pi/2$) magnetic fields of 20 G with different azimuths χ_B . These diagrams further highlight the large polarization amplitudes of the forward-scattering Hanle effect signals obtained in the PRD-AD setting. We find differences of approximately one order of magnitude (in both Q/I and U/I) when comparing PRD-AD with PRD-AA and CRD results. Much smaller, yet relevant, differences are instead found between the CRD and PRD-AA calculations. Consistently with the geometry of the problem, Q/I and U/I vanish for $\chi_B = \pi/4 + n\pi/2$ and $\chi_B = n\pi/2$ ($n = 0, \dots, 3$), respectively. It can be noticed that the evolution of the amplitudes of Q/I and U/I shows a counter-clockwise rotation in all cases. Interestingly, the line-center signal provided by CRD calculations always has the opposite sign

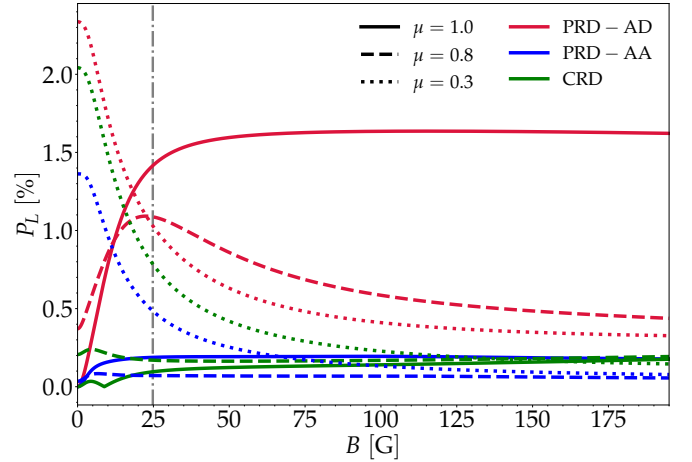


Fig. 4. Line-center linear polarization degree as a function of the strength of a horizontal ($\theta_B = \pi/2$, $\chi_B = 0$) magnetic field, obtained with PRD-AD (red), PRD-AA (blue) and CRD (green) calculations, for different LOSs. The vertical dash-dotted line indicates the Hanle critical field of Ca I 4227, that is $B_H = 25$ G.

with respect to the one provided by PRD-AA and PRD-AD calculations.

Figure 4 shows the line-center linear polarization degree

$$P_L = \frac{\sqrt{Q^2 + U^2}}{I}, \quad (1)$$

for different LOSs and magnetic field strengths of a horizontal magnetic field ($\theta_B = \pi/2$, $\chi_B = 0$), obtained with PRD-AD, PRD-AA, and CRD calculations. At the solar disk center ($\mu = 1$, solid lines), where the polarization is fully produced by the forward-scattering Hanle effect, P_L is already appreciable for

magnetic fields of a few gauss only. Its value quickly grows as the magnetic field strength increases further, and finally stabilizes above the Hanle critical field. The increase of P_L is much steeper and significant in the PRD-AD case than in the PRD-AA and CRD ones. Notably, the increase is not monotonic in the CRD case. As expected, for a near-limb LOS ($\mu = 0.3$, dotted lines), the Hanle effect produces a monotonic decrease of P_L with the magnetic field strength, until reaching a saturation regime. For an intermediate LOS ($\mu = 0.8$, dashed lines), the value of P_L first increases with the field strength, it reaches a maximum, and it finally decreases till the saturation regime. In the PRD-AD case, the initial increase is much steeper and significant, and the maximum is reached for stronger fields (around the Hanle critical field) than in the other cases. The PRD-AD calculations show significantly larger values of P_L for all LOS and for any magnetic field strength.

3.2. Inclined magnetic fields

The results presented in the previous section are obtained considering horizontal magnetic fields. This geometry maximizes the breaking of the axial symmetry for a given value of B , and thus the amplitude of the polarization signals produced at the disk center via the forward-scattering Hanle effect. On the other hand, the discrepancies between the emergent Stokes profiles resulting from PRD-AD, PRD-AA, and CRD calculations change significantly if magnetic fields with different inclinations with respect to the vertical are considered. For this reason, we now analyze the case of a non-horizontal inclined magnetic field. Figure 5 shows the center-to-limb variation of the amplitude of the line-center scattering polarization Q/I (upper panel) and U/I (lower panel) signals of the Ca I 4227 Å line, resulting from PRD-AD, PRD-AA, and CRD calculations in the presence of a height-independent inclined ($\theta_B = \pi/4$, $\chi_B = 0$) magnetic field of 20 G. This setting confirms the presence of relevant differences between the different scattering descriptions for all μ , and in particular for the forward-scattering geometry $\mu = 1$. To better visualize the impact of the different scattering modelings on the forward-scattering Hanle effect signal, Fig. 6 shows the emergent Q/I and U/I profiles at $\mu = 1$ for the same inclined magnetic field. Unlike in the case of a horizontal magnetic field shown in Fig. 2, this geometry produces an appreciable U/I signal. The significantly stronger linear polarization signals resulting from PRD-AD calculations are found both in Q/I and U/I .

Figure 7 compares the polarization diagrams for the line-center radiation emitted at $\mu = 1$ obtained with PRD-AD, PRD-AA and CRD calculations, considering height-independent inclined (i.e., $\theta_B = \pi/4$) magnetic fields of 20 G with different azimuths χ_B . These diagrams reveal smaller forward-scattering signals than those presented in Fig. 3, due to the smaller horizontal component of the 20 G magnetic field. Moreover, both the CRD and PRD-AA diagrams are rotated with respect to the PRD-AD one. This means that both approximations could lead to a wrong sign of the Q/I and U/I line-center signals. Figure 8 shows a similar polarization diagram, but for $\chi_B = 0$ and different inclinations θ_B of the 20 G magnetic field. As expected, the Q/I and U/I signals vanish in the presence of a vertical magnetic field, that is $\theta_B = 0, \pi$. As soon as the magnetic field is sufficiently inclined, the CRD and PRD-AA calculations significantly underestimate the amplitude of the line-center fractional linear polarization signals with respect to the PRD-AD modeling. Interestingly, the CRD diagram shows always negative line-center Q/I signals.

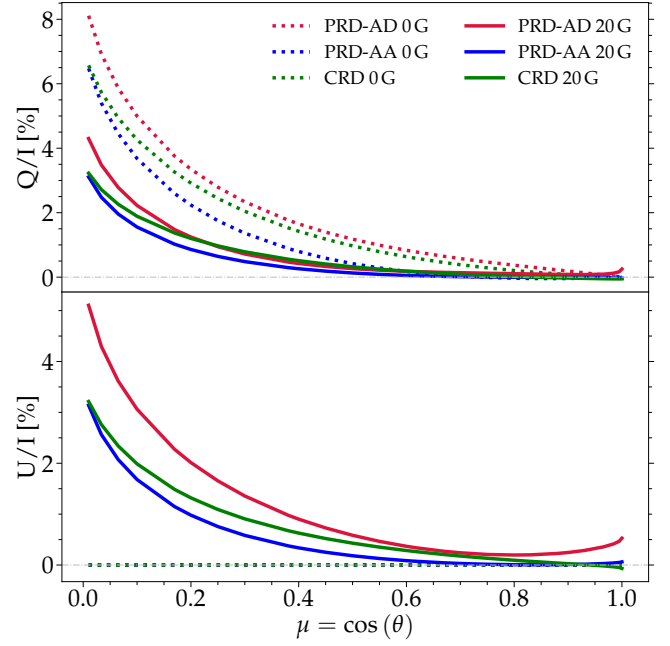


Fig. 5. Same as Fig. 1, but for a height-independent inclined ($\theta_B = \pi/4$, $\chi_B = 0$) magnetic field of 20 G.

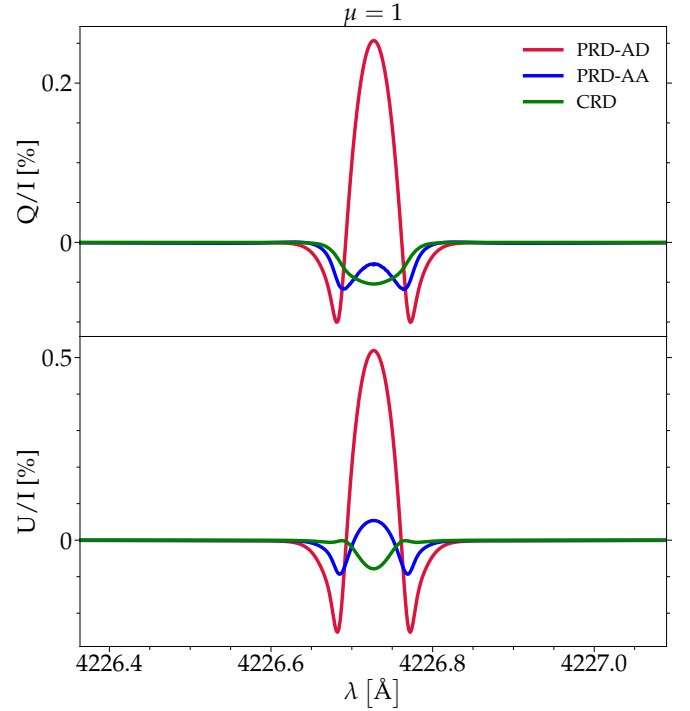


Fig. 6. Same as Fig. 2, but for a height-independent inclined ($\theta_B = \pi/4$, $\chi_B = 0$) magnetic field of 20 G.

4. Discussion

In general, CRD and PRD-AA calculations significantly underestimate the amplitude of the line-center fractional linear polarization signals, with respect to the PRD-AD modeling, and even the sign can be wrong. Providing a simple and intuitive inter-

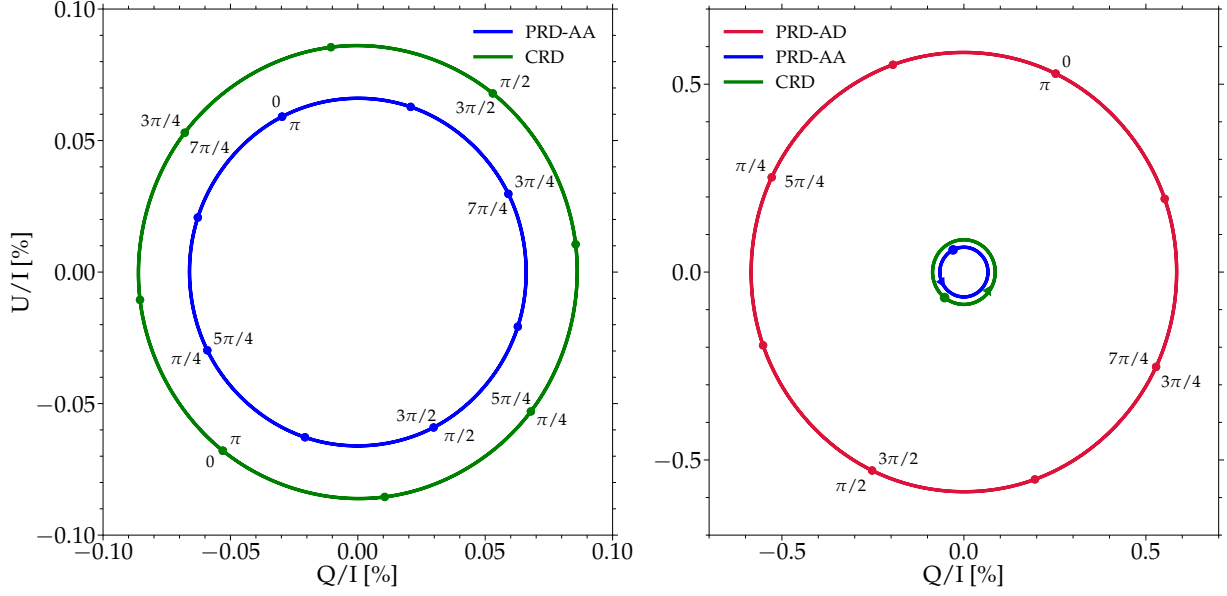


Fig. 7. Same as Fig. 3, but for a height-independent inclined ($\theta_B = \pi/4$) magnetic field of 20 G.

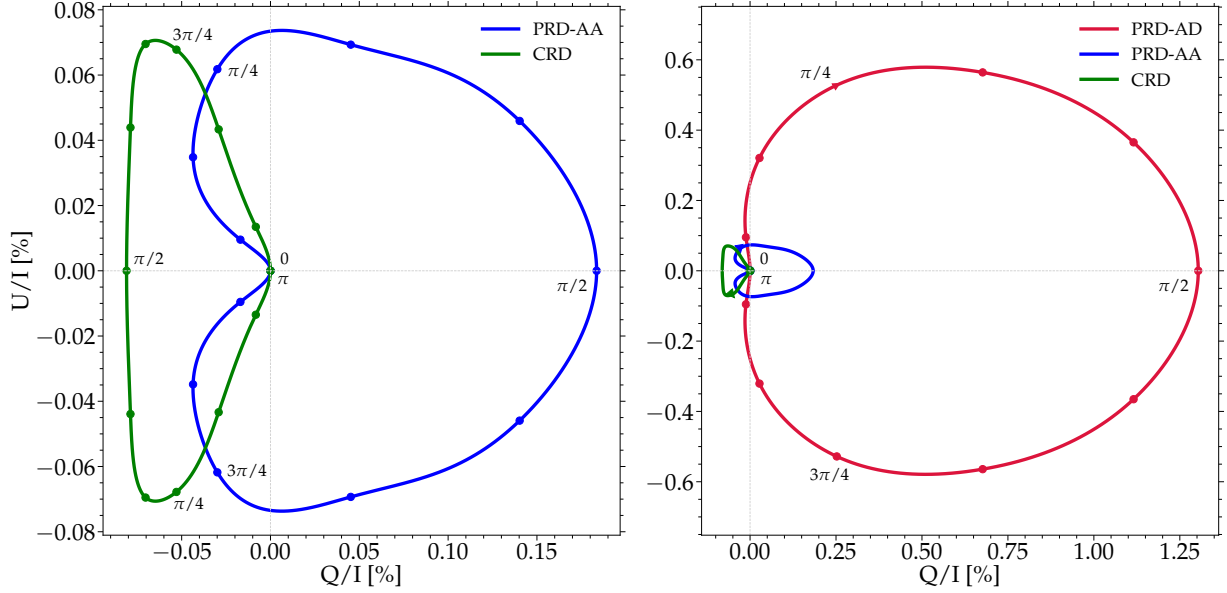


Fig. 8. Polarization diagrams obtained considering a height-independent magnetic field of 20 G with a fixed azimuth $\chi_B = 0$, and varying its inclination $\theta_B \in [0, \pi]$. The circular markers indicate the effective calculations, carried out for $\theta_B = n\pi/12$ with $n = 0, \dots, 12$. The other parameters are the same as in Fig. 3.

pretation of these results is, unfortunately, not straightforward. Here, we provide a few qualitative insights.

The polarization properties of scattered radiation strongly depend on the detailed spectral and angular dependencies of the incident radiation field. These dependencies can only be fully taken into account through a PRD-AD description of scattering processes, while they are necessarily smoothed by the averages inherent to the PRD-AA and CRD approximations. Indeed, it can be shown that the CRD, PRD-AA, and PRD-AD calculations coincide in the limit of a spectrally flat and isotropic radiation field. It appears reasonable that scattering polarization signals, which are ultimately due to the geometry of the problem and symmetry-breaking effects, are enhanced by the PRD-

AD approach, which exactly accounts for the complex coupling between the frequencies and propagation directions of the incoming and scattered radiation. Besides, the particular spectral structure and anisotropy of the solar radiation field depend on the thermal and density stratification of the atmospheric model through non-local RT effects. Inspecting and predicting these effects in non-academic scenarios is notoriously difficult, and an even more complex task is to predict how they are impacted by the considered approximations in the modeling of scattering processes. In conclusion, it is not possible to clearly identify a single specific reason that explains the large differences observed between the CRD or PRD-AA calculations with respect to the general PRD-AD modeling. Nonetheless, these results clearly

manifest the necessity of considering PRD effects in their general AD formulation. This fact is even more crucial for full 3D RT calculations, which consider the detailed geometrical structure of the solar plasma. At the dawn of the new generation of the big solar spectropolarimetric facilities like the Daniel K. Inouye Solar Telescope (DKIST, Rimmele et al. 2020) and the future European Solar Telescope (EST, Quintero Noda et al. 2022), the call to fully include the physical processes affecting the polarization of spectral lines is indeed stronger than ever before.

A last remark concerns the significant discrepancies between the theoretical calculations presented in Sect. 3.1, which predict polarization signals around 1 %, and the observations of Bianda et al. (2011), which show signals one order of magnitude weaker (around 0.1 %). This difference is not surprising, noticing that a horizontal magnetic field maximizes the breaking of the axial symmetry and thus the forward-scattering Hanle effect. Moreover, the 3D calculations in the CRD limit by Jaume Bestard et al. (2021) indicate that the presence of an inclined magnetic field reduces (and does not enhance) the amplitude of the scattering polarization signals produced by both horizontal inhomogeneities of the solar plasma and spatial gradients of the plasma bulk velocity (which are neglected in this work). The inclusion of mechanisms (i) and (ii) and the use of state-of-the-art 3D MHD atmospheric models are needed to obtain reliable information on the magnetic field strength. We also note that the impact of instrumental effects on the observed line-core signals is significant, especially in forward scattering observations (e.g., Zeuner et al. 2020; del Pino Alemán & Trujillo Bueno 2021, for the Sr I 4607 Å line).

5. Conclusions

The results of this work show that a reliable modeling of the fractional linear polarization signals produced through the forward-scattering Hanle effect in the Ca I line at 4227 Å requires taking PRD effects into account in their general AD formulation. If the CRD or PRD-AA approximations are considered, the amplitude of the line-center Q/I and U/I signals close to $\mu = 1$ could be significantly underestimated, and even the sign can be wrong. This finding is of clear relevance, especially for the development of new methods for solar magnetic field diagnostics based on forward-scattering polarization signals in the Ca I 4227 Å line.

It can be expected that the results presented here for the Ca I 4227 Å line generalize to other strong resonance lines, for which PRD effects are relevant. For this reason, it is important to extend this work to other spectral lines of interest for Hanle diagnostics, such as those recently observed by the CLASP experiments (e.g., Kano et al. 2017; Rachmeler et al. 2022), or those that DKIST (and EST) will allow observing with unprecedented spatial and temporal resolutions.

Finally, it will be of high interest to consider realistic 3D atmospheric models, which allow including horizontal inhomogeneities of the solar plasma and spatial gradients of the bulk velocity. In this respect, the first 3D non-LTE RT calculations, taking scattering polarization and AD PRD effects into account, will soon be available thanks to recent software and algorithmic developments (see Benedusi et al. 2023).

Acknowledgements. This work was financed by the Swiss National Science Foundation (SNSF) through grant CRSII5_180238. T.P.A.'s participation in the publication is part of the Project RYC2021-034006-I, funded by MICIN/AEI/10.13039/501100011033, and the European Union "NextGenerationEU"/RTRP. T.P.A., J.T.B. and E.A.B. acknowledge support from the Agencia Estatal de Investigación del Ministerio de Ciencia, Innovación y Universidades (MCIU/AEI) under grant "Polarimetric Inference of Magnetic Fields" and

the European Regional Development Fund (ERDF) with reference PID2022-136563NB-I00/10.13039/501100011033. J.Š. acknowledges the financial support from project RVO:67985815 of the Astronomical Institute of the Czech Academy of Sciences.

References

- Alsina Ballester, E., Belluzzi, L., & Trujillo Bueno, J. 2018, *ApJ*, 854, 150
- Anusha, L. S., Nagendra, K. N., Bianda, M., et al. 2011, *ApJ*, 737, 95
- Benedusi, P., Janett, G., Belluzzi, L., & Krause, R. 2021, *A&A*, 655, A88
- Benedusi, P., Janett, G., Riva, S., Krause, R., & Belluzzi, L. 2022, *A&A*, 664, A197
- Benedusi, P., Riva, S., Zulian, P., et al. 2023, *Journal of Computational Physics*, 479, 112013
- Bianda, M., Ramelli, R., Anusha, L. S., et al. 2011, *A&A*, 530, L13
- Bommier, V. 1997a, *A&A*, 328, 706
- Bommier, V. 1997b, *A&A*, 328, 726
- Carlin, E. S. & Bianda, M. 2016, *ApJ*, 831, L5
- Carlin, E. S. & Bianda, M. 2017, *ApJ*, 843, 64
- del Pino Alemán, T. & Trujillo Bueno, J. 2021, *ApJ*, 909, 180
- del Pino Alemán, T., Trujillo Bueno, J., Casini, R., & Manso Sainz, R. 2020, *ApJ*, 891, 91
- del Pino Alemán, T., Trujillo Bueno, J., Štěpán, J., & Shchukina, N. 2018, *ApJ*, 863, 164
- Faurobert, M. 1988, *A&A*, 194, 268
- Fontenla, J. M., Avrett, E. H., & Loeser, R. 1993, *ApJ*, 406, 319
- Gandorfer, A. 2000, *The Second Solar Spectrum: A high spectral resolution polarimetric survey of scattering polarization at the solar limb in graphical representation. Volume I: 4625 Å to 6995 Å* (Zurich: vdf ETH)
- Gandorfer, A. 2002, *The Second Solar Spectrum: A high spectral resolution polarimetric survey of scattering polarization at the solar limb in graphical representation. Volume II: 3910 Å to 4630 Å* (Zurich: vdf ETH)
- Gandorfer, A. 2005, *The Second Solar Spectrum: A high spectral resolution polarimetric survey of scattering polarization at the solar limb in graphical representation. Volume III: 3160 Å to 3915 Å* (Zurich: vdf ETH)
- Guerreiro, N., Janett, G., Riva, S., Benedusi, P., & Belluzzi, L. 2024, *A&A*, 683, A207
- Janett, G., Alsina Ballester, E., Guerreiro, N., et al. 2021a, *A&A*, 655, A13
- Janett, G., Benedusi, P., Belluzzi, L., & Krause, R. 2021b, *A&A*, 655, A87
- Janett, G., Benedusi, P., & Riva, F. 2024, *A&A*, 682, A68
- Jaume Bestard, J., Trujillo Bueno, J., Štěpán, J., & del Pino Alemán, T. 2021, *ApJ*, 909, 183
- Kano, R., Trujillo Bueno, J., Winebarger, A., et al. 2017, *ApJ*, 839, L10
- Landi Degl'Innocenti, E. & Landolfi, M. 2004, *ASSL*, Vol. 307, *Polarization in Spectral Lines* (Dordrecht: Kluwer), [LL04]
- Manso Sainz, R. & Trujillo Bueno, J. 2011, *ApJ*, 743, 12
- Quintero Noda, C., Schlichenmaier, R., Bellot Rubio, L. R., et al. 2022, *A&A*, 666, A21
- Rachmeler, L. A., Trujillo Bueno, J., McKenzie, D. E., et al. 2022, *ApJ*, 936, 67
- Ramelli, R., Balemi, S., Bianda, M., et al. 2010, in *SPIE Conf. Ser.*, Vol. 7735, *Ground-based and Airborne Instrumentation for Astronomy III*, ed. I. S. McLean, S. K. Ramsay, & H. Takami, 77351Y
- Rimmele, T. R., Warner, M., Keil, S. L., et al. 2020, *Solar Physics*, 295, 172
- Riva, S., Guerreiro, N., Janett, G., et al. 2023, *A&A*, 679, A87
- Sampoorna, M., Nagendra, K. N., & Stenflo, J. O. 2017, *ApJ*, 844, 97
- Sampoorna, M., Trujillo Bueno, J., & Landi Degl'Innocenti, E. 2010, *ApJ*, 722, 1269
- Stenflo, J. O. 2003, in *ASP Conf. Ser.*, Vol. 307, *Solar Polarization*, ed. J. Trujillo Bueno & J. Sanchez Almeida, 385
- Stenflo, J. O. & Keller, C. U. 1997, *A&A*, 321, 927
- Trujillo Bueno, J. 2001, in *ASP Conf. Ser.*, Vol. 236, *Advanced Solar Polarimetry – Theory, Observation, and Instrumentation*, ed. M. Sigwarth, 161
- Trujillo Bueno, J. & del Pino Alemán, T. 2022, *ARA&A*, 60, 415
- Trujillo Bueno, J., Landi Degl'Innocenti, E., Collados, M., Merenda, L., & Manso Sainz, R. 2002, *Nature*, 415, 403
- Uitenbroek, H. 2001, *ApJ*, 557, 389
- Štěpán, J. & Trujillo Bueno, J. 2013, *A&A*, 557, A143
- Štěpán, J. & Trujillo Bueno, J. 2016, *ApJ*, 826, L10
- Zeuner, F., Manso Sainz, R., Feller, A., et al. 2020, *ApJ*, 893, L44